❒ 1080

Wideband and high gain mmWave antenna with phase gradient metasurface

Devendra Soni, Dinesh Yadav, Manish Tiwari
Department of Electronics and Communication Engineering (ECE), Manipal University Jaipur, Jaipur, India

Article Info

ABSTRACT

This study presents a phase gradient metasurface (PGM) measuring 30 mm on each side and discusses its development. The use of multiple unit cell sizes is critical to the design of the PGM that was produced. A sand-timer-shaped monopole antenna was designed specifically for wideband millimetre wave (mmWave) applications. An antenna structure is reinforced with a PGM that was specifically designed to increase antenna gain over its bandwidth. This is done to increase the antenna gain overall. The antenna has a bandwidth of 9.18 GHz, which includes mmWave frequencies ranging from 20.78 GHz to 29.96 GHz. For a wideband response, the ground plane must contain flaws. These flaws must exist on the surface of the ground plane. This study presents an in-depth examination of the antenna, PGM design, and operating principles, backed up by experimental verification. The use of PGM results in a 5 dB increase in antenna gain, with an average improvement of 2 dBi across all frequencies.

Corresponding Author:

Dinesh Yadav
Department of Electronics and Communication Engineering (ECE), Manipal University Jaipur
Jaipur, India
Email: dinesh.yadav@jaipur.manipal.edu

1. INTRODUCTION

Antennas serve a vital role in both receiving and sending waves. Higher data rates are required due to the rising traffic in social networking, cloud-based computing, e-commerce, and online video streaming [1]. The currently operating 4G wireless network is experiencing a limit of capacity. It might not be able to handle the rising data demand, so interest has been shifted to the millimeter wave frequencies [2]. The Federal Communications Commission (FCC) for mmWave 5G communications has classified the 20-50 GHz frequency band as K-band, Ka-band, and some V-band [3]. Millimetre wave (mmWave) frequency spectrum at the 28 GHz band offers wide bandwidth and low latency. It finds applications in various communication fields that offer less atmospheric attenuation, low path loss, and low signal spread [4].

The configuration of the unit cell within a two-dimensional plane is referred to as a metasurface. With the advent of metamaterials towards the close of the 20th century, the design ideas and uses of materials have been greatly increased [5]. The two-dimensional extension of the metamaterials idea known as metasurface (MS) has made it possible to manipulate electromagnetic (EM) waves with previously unheard-of freedom [6]. The substantial applications of MS, such as holographic imaging [7], vortex beam generators [8], surface plasmon metacouplers [9], versatile MS [10], and lenses [11], [12], are a result of these merits.

A subfield of MS called phase gradient metasurface (PGM) has yielded a number of beneficial applications, including refraction or abnormal refraction [13], [14], decrease of radar cross-section (RCS) [15], [16], focusing EM [17], [18], and polarization beam splitter (PBS) [19], [20]. To demonstrate generalized Snell's law [21] and show that phase discontinuities may be exploited to create MS,

Yu *et al.* [22] initially used the PGM by putting forward a V-shaped nano-antenna. Since then, PGM has been extensively used in a variety of settings, including the microwave and optical bands [23], [24].

As the application range has grown, more PGMs have been developed. Traditional reflecting PGMs are not the recommended PGMs since they will block reflected EM waves and increase return loss [25], [26]. Transmissive PGMs make it more practical to increase the antenna's gain in circumstances when mounting the feed antenna on the MS's back is not appropriate. Nevertheless, while developing transmissive PGMs, the transmission amplitude and phase must be considered simultaneously, increasing the design's complexity [27], [28]. Zhong *et al.* [29] phase-shifting surface, whose back is made up of a frequency-selective surface (FSS), may function as a transmit array at high frequencies and a reflect array at low frequencies. A PGM array that is composed of a transmissive PGM, a reflecting PGM, and an FSS is presented in [30]. This array produces a beam that is focused at two distinct frequencies and in two directions. Typically, the single frequency and single radiation direction of typical PGM antenna systems are their drawbacks. While certain antennas can produce dual-frequency and dual-mode radiation, reflecting PGMs or FSS are entirely responsible for the reflection features.

The proposed method achieves broad response at mmWave frequencies by employing a simple microstrip line fed sand-timer shaped antenna with defective ground structure (DGS). The antenna has a broad bandwidth of 9.18 GHz, spanning from 20.78 GHz to 29.96 GHz. A tailored PGM mounted over the antenna boosts the antenna's gain. The antenna gain is boosted from 5 dBi to more than 7 dBi throughout the operating range.

2. DESIGN AND DISCUSSION

A square-shaped PGM with dimensions of 30×30 mm has been created. The PGM consists of a grid of 9×9-unit cells, which are also engraved on the upper surface of the FR-4 substrate. The substrate has a thickness of 3.2 mm and is arranged in a modified sand-timer shape. The substrate material has a relative permittivity (ε_r) of 4.4 and a loss tangent ($tan\,\delta$) of 0.025.

The antenna under consideration consists of a patch with a sand-timer form that is etched onto the upper surface of a Rogers/RT-Duroid 5880 substrate. The substrate has a thickness of 0.8 mm and possesses a relative permittivity (ε_r) of 2.2, as well as a loss tangent ($tan\,\delta$) of 0.009. The patch is fed via a microstrip line that incorporates ground plane defects. The antenna under consideration has been optimized for operation within the millimeter wave frequency range spanning from 20 GHz to 30 GHz.

The implemented probabilistic model of PGM is positioned in proximity to the antenna to enhance the overall gain of the antenna. Figure 1(a) illustrates the proposed antenna geometry, while Figure 1(b) portrays the suggested PGM geometry. Lastly, Figure 1(c) presents the combined geometry of the antenna and PGM. Tables 1 and 2 present the comprehensive compilation of the optimized design parameters for both the antenna and the PGM.
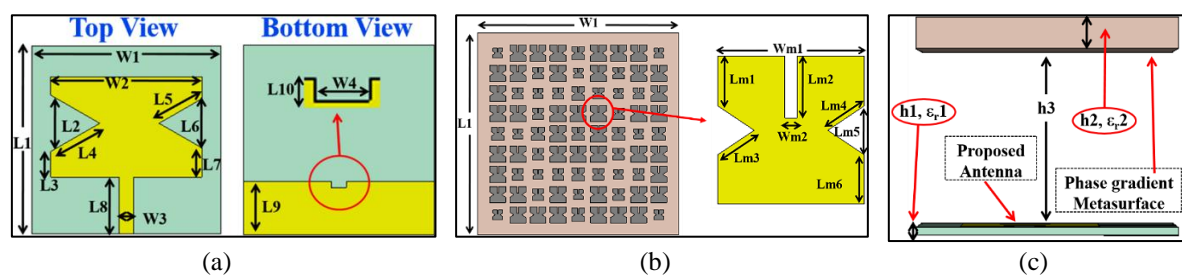

| (a) | (b) | (c) |

Figure 1. Probabilistic of PGM; (a) antenna geometry, (b) PGM, and (c) PGM placement over the antenna

Table 1. List of design parameters of the antenna

Variable	Value (mm)	Variable	Value (mm)
L1	30	L9	8.5
L2	9	L10	1
L3	4.1	W1	30
L4	9	W2	24
L5	7.85	W3	2.37
L6	7.85	W4	2.37
L7	4.67	h1	0.8
L8	9	ε_r1	2.2 (unitless)

Table 2. List of design parameters of PGM

Variable	Value (mm)
Lm1	0.8
Lm2	1
Lm3	0.72
Lm4	0.72
Lm5	0.8
Lm6	0.8
Wm1	2.4
Wm2	0.2
h2	3.2
h3	9.2
$\varepsilon_r 2$	4.4 (unitless)

The antenna under consideration is based on a microstrip line-fed rectangular patch antenna, and its progressive development will be elaborated upon in this discourse. The process of design evolution consists of three distinct steps, denoted step-1, step-2, and step-3, as depicted in Figure 2(a). The primary aim of implementing design improvements, which encompass addressing flaws in the ground plane, is to attain a broad bandwidth. Consequently, the antenna has a bandwidth of 9.07 GHz, commencing at 20.78 GHz and extending to 29.96 GHz. Figure 2(b) presents the findings of a comparison analysis conducted on the results of design evolution.
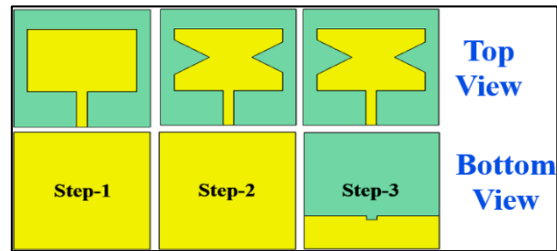
(a)
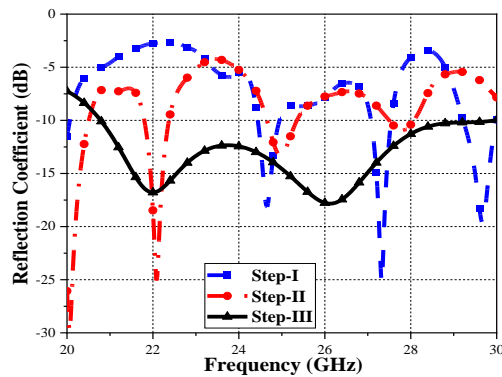
(b)

Figure 2. The evolution of the antenna and its comparison is shown in; (a) antenna evolution stages and (b) reflection coefficient plot

After being analyzed to provide an additional physical perspective on the antenna design, the current distribution is depicted in Figure 3 showing how it behaves at a variety of frequencies. The two resonance frequencies of the design, which are 22 GHz represented in Figure 3(a) and 26 GHz represented in Figure 3(b), were chosen to be the selected frequencies. The two resonance frequencies of the design, which are 22 GHz and 26 GHz, were chosen to be the selected frequencies. Depending on the frequency that is chosen, there will be a variety of different current distributions at each one. It has been observed that the current may be traced back and forth between the patch, the feed line, and the ground plane. Figure 4 illustrates the systematic current distribution on the PGM at specific frequency points, namely 22 GHz as

shown in Figure 4(a) and 26 GHz as in Figure 4(b). Based on the observed current patterns, it is evident that there is a circulation of current on every cell of the metasurface.
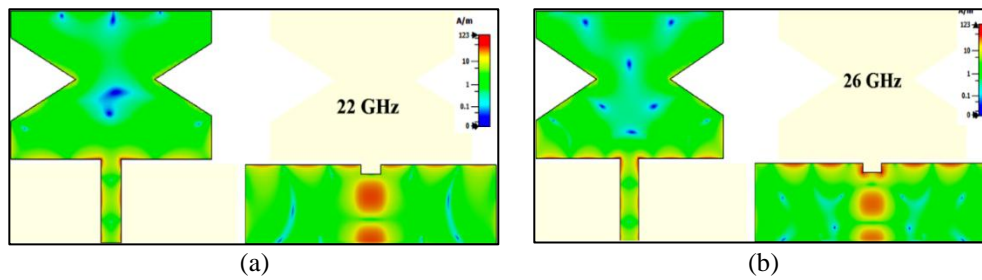

(a)   (b)

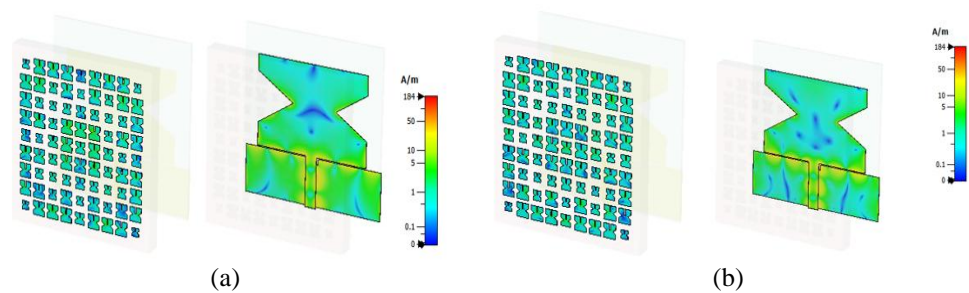Figure 3. Surface current distribution on antenna at; (a) 22 GHz and (b) 26 GHz

(a)   (b)

Figure 4. Surface current distribution on PGM at; (a) 22 GHz and (b) 26 GHz

The plot between the antenna's gain and frequency is depicted in the top part of Figure 5(a). The gain, despite displaying a change of approximately 5 dB, is observed to stay steady over the impedance bandwidth of the antenna. This is a consistent observation that has been made. An increase in antenna gain over the impedance bandwidth can be achieved with the help of a phased gradient metasurface, also known as PGM. After applying the PGM, it is immediately noticeable that the gain of the antenna has been increased by 5 dB as a result of the adjustment. The antenna design displays an aggregate gain that is greater than 7 dB over the range of frequencies that have been specified. The optimization of antenna gain throughout a broad operational bandwidth is made easier by the favorable arrangement of a large number of zero reflection points close to one another. The data that is shown in Figure 5(b) shows that the performance of the antenna is unaffected by the positioning of the PGM about the reflection coefficient. This is the conclusion that can be drawn from the information. The use of the PGM not only kept the antenna's operational bandwidth stable but also resulted in an improvement in the gain performance of the antenna.

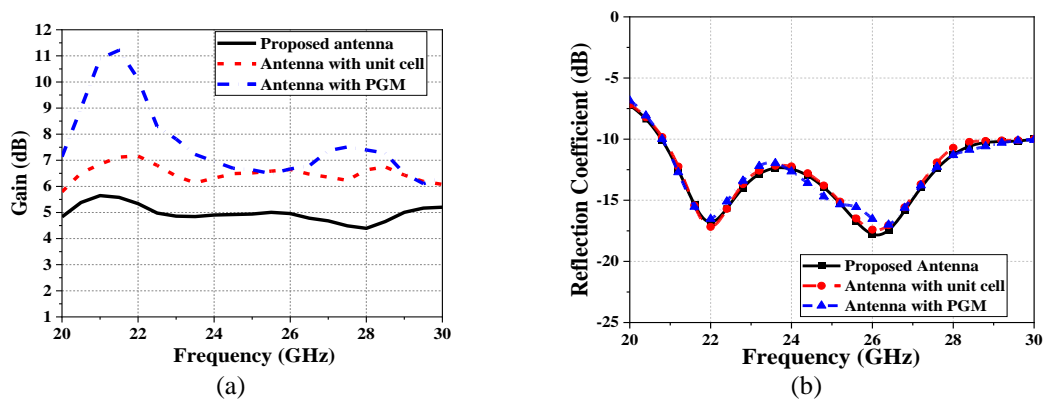(a)   (b)

Figure 5. The plot antenna is depicted at; (a) gain versus frequency plot and (b) reflection coefficient plot

The optimization of the space between the antenna and the PGM is done to get maximum gain over the antenna bandwidth while still maintaining the antenna bandwidth. This is done by optimizing the space between the antenna and the PGM. Figure 6 illustrates the fluctuation in gain that occurs inside the system as a result of a change in the distance that exists between the antenna and the PGM. The pattern that has been observed suggests that the total gain of the design will initially grow when the distance between the PGM and antenna (h3) is extended. However, once it reaches a certain threshold, it will begin to decline and will continue to do so beyond that point. The value of h3 was determined to be 9.2 millimetersto achieve the highest possible gain through optimization.
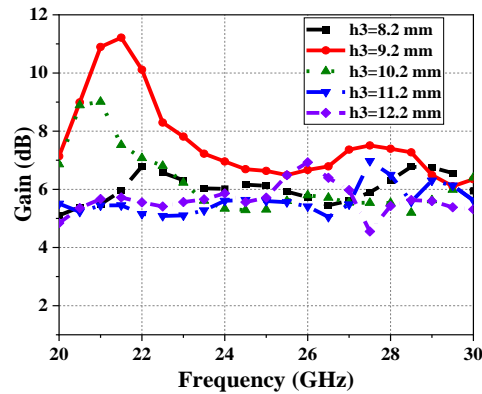

Figure 6. Effect of varying distance between antenna and PGM on the antenna gain

3. MEASUREMENT RESULTS

Figure 7 is an illustration of the constructed prototype of the antenna with the PGM affixed to it. Figure 7(a) presents proposed antenna, Figure 7(b) depicts PGM structure, Figure 7(c) portrays proposed antenna with PGM, and Figure 7(d) shows measurement setup in an anechoic chamber. To obtain the desired level of separation between the antenna and the PGM during the prototype fabrication process, plastic spacers of the appropriate proportions are used.

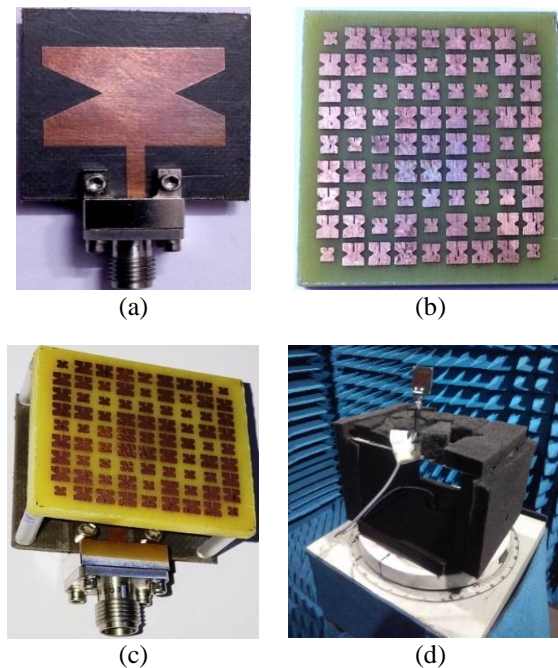(a)   (b)

(c)   (d)

Figure 7. Illustration of the constructed prototype of the antenna; (a) proposed antenna, (b) PGM structure, (c) proposed antenna with PGM, and (d) measurement setup in an anechoic chamber

The examination of Figure 8 demonstrates that the simulated bandwidth extends from 20.78 GHz to 29.96 GHz, but the measured bandwidth extends from 20.9 GHz to 28.8 GHz. The differences that were observed between the simulated data and the measured data could perhaps be ascribed to flaws in the fabrication process or the soldering. Measured reflection coefficient results are presented in Figure 8. Figure 8(a) illustrates reflection coefficients results without using PGM whereas Figure 8(b) represents reglection coefficient results by using PGM.
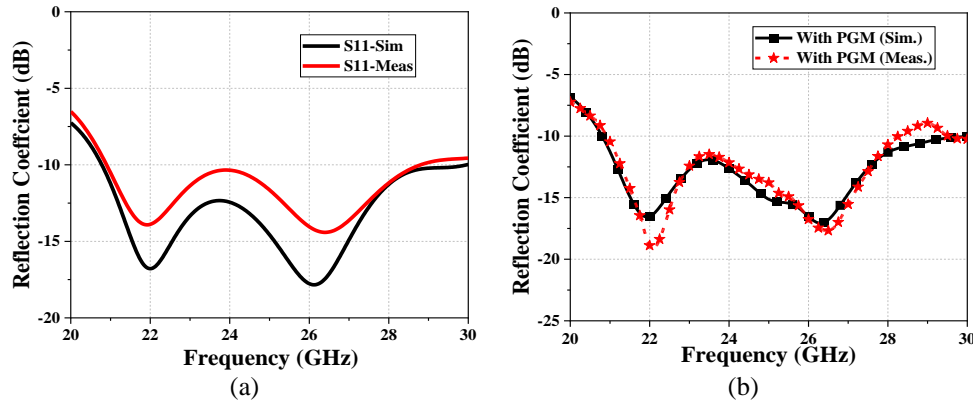

Figure 8. Measured reflection coefficient results; (a) without PGM and (b) with PGM

Figure 9 provides a visual representation of the gain comparison, which demonstrates how consistent the design's gain is over the target band. The validity of this observation has been verified by experimental verification. Figure 9(a) represents gain comparison without PGM and Figure 9(b) illustrates gain comparison with PGM.
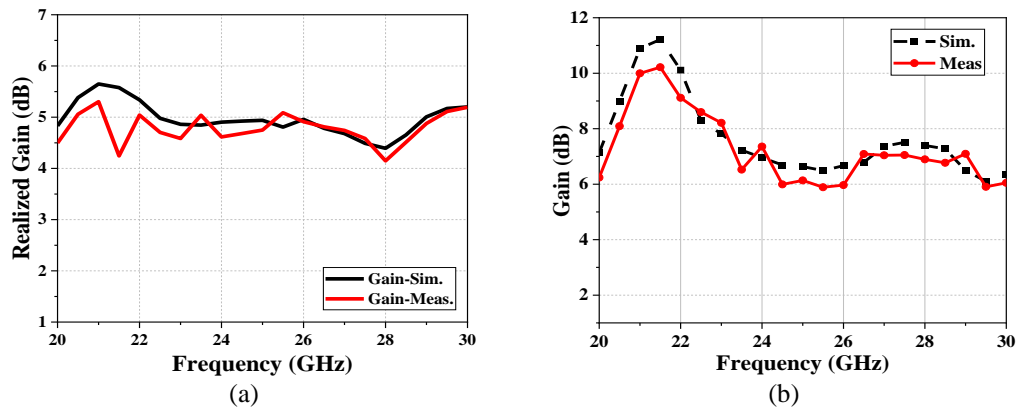

Figure 9. Gain comparison at; (a) without the PGM and (b) with the PGM mounted on the antenna

Figure 10 depicts the radiation patterns that the suggested antenna design would produce if it were optimized for the strong resonances of the operational bands. Figure 10(a) represents radiation patterns at 22 GHz and Figure 10(b) represents radiation patterns at 26 GHz. The receiver was fitted with a proposed antenna, in contrast to the usual pyramidal Horn antenna that was installed in the transmitter. The discovered patterns demonstrate a high degree of omnidirectionality throughout the whole spectrum of frequencies that were investigated. The generated data and the measured data are quite comparable to the observed patterns, which shows that the patterns are very accurate. The antenna is evaluated by other antennas discussed in the existing literature in terms of its efficacy and potential for improvement. The comparative analysis is depicted in Table 3. The design being suggested exhibits the smallest physical dimensions ($2.07 \lambda 0 \times 2.07 \lambda 0$), offers a broader range of frequencies for operation (9.18 GHz) and achieves a level of gain that is either comparable to or surpasses the performance of similar structures documented in existing scholarly works.

The implementation of a PGM at an appropriate distance yields an enhancement in antenna gain while preserving the integrity of other performance characteristics associated with the antenna.
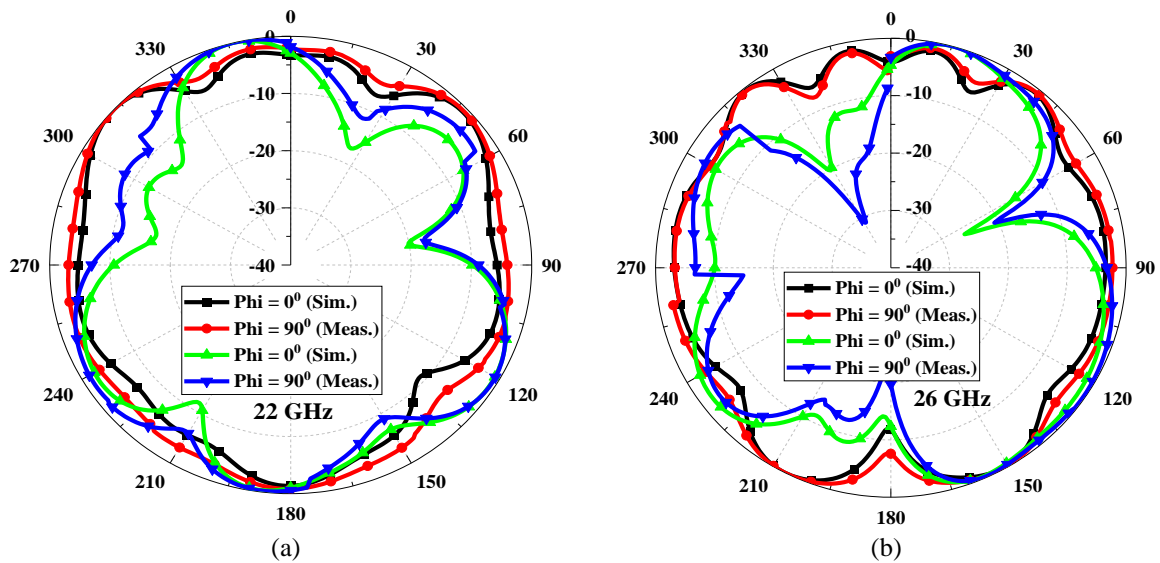

Figure 10. Radiation patterns at; (a) 22 GHz and (b) 26 GHz

Table 3. Comparison with the other published work

Ref.	Method for gain improvement	Operating frequency (GHz)	Antenna gain (dB)	Area of antenna (calculated at lower cutt-off frequency) (λ_0)	Distance between antenna and PGM (λ_0)
[15]	H shape resonator	2.2–3.9	7.4	0.58×0.51	0.076
[16]	Multi-layered split ring resonator	5.6–7.8	10.2	1.40×0.69	0.086
[17]	Frequency selective surface	7.6	7.22	1.62×1.62	0.891
[18]	Double ring element based lens	6	16.7	4.2×4.2	4.6
[19]	Plastic lens superstrate	5.8	10	1×1	0.549
[20]	PGM	17.1	16.5	7.4×7.4	2.366
[22]	PGM	28	12.4	4.66×4.66	1.866
Here	PGM	20.78–29.96	7 - 11	2.07×2.07	0.637

4. CONCLUSION

The paper presents an analysis of a cost-effective methodology aimed at enhancing the gain of microstrip patch-based antennas in the context of wideband mmWave applications. The antenna has a broad frequency range of 9.18 GHz (20.78 GHz to 29.96 GHz) inside the 28 GHz mmWave frequency band. The antenna has a gain of 5 dB, which remains rather constant across the whole bandwidth of the antenna. The implementation of a PGM in a strategically designed configuration has been found to significantly enhance the antenna gain, resulting in an improvement of up to 11 dBi. The current landscape of broadband 5G communication applications presents an opportunity for the utilization of a compact, planar, and straightforward antenna design that boasts a low profile. This design also has the advantage of high gain and ease of manufacture, further enhancing its suitability for such applications.

REFERENCES

[1] S. Kumar, A. S. Dixit, R. R. Malekar, H. D. Raut, and L. K. Shevada, "Fifth Generation Antennas: A Comprehensive Review of Design and Performance Enhancement Techniques," in *IEEE Access*, vol. 8, pp. 163568-163593, 2020, doi: 10.1109/ACCESS.2020.3020952.

[2] P. Shariff, P. R. Manea, P. Kumarb, T. Alia, and M. G. N. Alsathc, "Planar MIMO antenna for mmWave applications: Evolution, present status & future scope," *Heliyon*, vol. 9, no. 2, p. e13362, Feb. 2023, doi: 10.1016/j.heliyon.2023.e13362.

[3] N. K. Mallat, M. Ishtiaq, A. Ur Rehman, and A. Iqbal, "Millimeter-Wave in the Face of 5G Communication Potential Applications," *IETE Journal of Research*, vol. 68, no. 4, pp. 2522-2530, Jan. 2020, doi: 10.1080/03772063.2020.1714489.

[4] R. Ford, M. Zhang, M. Mezzavilla, S. Dutta, S. Rangan, and M. Zorzi, "Achieving Ultra-Low Latency in 5G Millimeter Wave Cellular Networks," in *IEEE Communications Magazine*, vol. 55, no. 3, pp. 196-203, March 2017, doi: 10.1109/MCOM.2017.1600407CM.

[5] B. Luk'yanchuk *et al.*, "The Fano resonance in plasmonic nanostructures and metamaterials," *Nature Materials*, vol. 9, no. 9, pp. 707–715, Sep. 2010, doi: 10.1038/nmat2810.

[6] J. Wang *et al.,* "Metantenna: When Metasurface Meets Antenna Again," in *IEEE Transactions on Antennas and Propagation*, vol. 68, no. 3, pp. 1332-1347, Mar. 2020, doi: 10.1109/TAP.2020.2969246.

[7] M. F. Imani *et al.,* "Review of Metasurface Antennas for Computational Microwave Imaging," in *IEEE Transactions on Antennas and Propagation*, vol. 68, no. 3, pp. 1860-1875, March 2020, doi: 10.1109/TAP.2020.2968795.

[8] B. He, J. Fan, Y. Cheng, F. Chen, H. Luo, and R. Gong, "Thermally tunable terahertz vortex beam generator based on an InSb metasurface," *Journal of the Optical Society of America B*, vol. 38, no. 5, pp. 1518–1524, May 2021, doi: 10.1364/JOSAB.420928.

[9] W. Sun, Q. He, S. Sun, and L. Zhou, "High-efficiency surface plasmon meta-couplers: concept and microwave-regime realizations," *Light: Science & Applications*, vol. 5, no. 1, p. e16003, Jan. 2016, doi: 10.1038/lsa.2016.3.

[10] P. Fei *et al.,* "Versatile Cross-Polarization Conversion Chiral Metasurface for Linear and Circular Polarizations," *Advanced Optical Materials*, vol. 8, no. 13, May 2020, doi: 10.1002/adom.202000194.

[11] H. Cheng, H. Yang, Y. Li, and Y. Chen, "A Compact Vivaldi Antenna with Artificial Material Lens and Sidelobe Suppressor for GPR Applications," in *IEEE Access*, vol. 8, pp. 64056-64063, 2020, doi: 10.1109/ACCESS.2020.2984010.

[12] E. Zhou, Y. Cheng, F. Chen, and H. Luo, "Wideband and high-gain patch antenna with reflective focusing metasurface," *AEU - International Journal of Electronics and Communications,* vol. 134, p. 153709, 2021, doi: 10.1016/j.aeue.2021.153709.

[13] K. Singh, M. U. Afzal, M. Kovaleva, and K. P. Esselle, "Controlling the Most Significant Grating Lobes in Two-Dimensional Beam-Steering Systems with Phase-Gradient Metasurfaces," in *IEEE Transactions on Antennas and Propagation*, vol. 68, no. 3, pp. 1389-1401, March 2020, doi: 10.1109/TAP.2019.2955244.

[14] H. Shi *et al.,* "Gradient Metasurface with Both Polarization-Controlled Directional Surface Wave Coupling and Anomalous Reflection," in *IEEE Antennas and Wireless Propagation Letters*, vol. 14, pp. 104-107, 2015, doi: 10.1109/LAWP.2014.2356483.

[15] F. Yuan, G.-M. Wang, H.-X. Xu, T. Cai, X.-J. Zou, and Z.-H. Pang, "Broadband RCS Reduction Based on Spiral-Coded Metasurface," in *IEEE Antennas and Wireless Propagation Letters*, vol. 16, pp. 3188-3191, 2017, doi: 10.1109/LAWP.2017.2768129.

[16] T. V. Hoang, C.-H. Lee, and J.-H. Lee, "Two-Dimensional Efficient Broadband Retrodirective Metasurface," in *IEEE Transactions on Antennas and Propagation*, vol. 68, no. 3, pp. 2451-2456, March 2020, doi: 10.1109/TAP.2019.2940501.

[17] T. Cai, G.-M. Wang, X.-L. Fu, J.-G. Liang, and Y.-Q. Zhuang, "High-Efficiency Metasurface with Polarization-Dependent Transmission and Reflection Properties for Both Reflectarray and Transmitarray," in *IEEE Transactions on Antennas and Propagation*, vol. 66, no. 6, pp. 3219-3224, June 2018, doi: 10.1109/TAP.2018.2817285.

[18] H. Li, G. Wang, J. Liang, X. Gao, H. Hou, and X. Jia, "Single-Layer Focusing Gradient Metasurface for Ultrathin Planar Lens Antenna Application," in *IEEE Transactions on Antennas and Propagation*, vol. 65, no. 3, pp. 1452-1457, March 2017, doi: 10.1109/TAP.2016.2642832.

[19] T. Cai *et al.,* "Ultra-Thin Polarization Beam Splitter Using 2-D Transmissive Phase Gradient Metasurface," in *IEEE Transactions on Antennas and Propagation*, vol. 63, no. 12, pp. 5629-5636, Dec. 2015, doi: 10.1109/TAP.2015.2496115.

[20] L. Bao *et al.,* "Multi-Beam Forming and Controls by Metasurface with Phase and Amplitude Modulations," in *IEEE Transactions on Antennas and Propagation*, vol. 67, no. 10, pp. 6680-6685, Oct. 2019, doi: 10.1109/TAP.2019.2925289.

[21] F. Aieta *et al.,* "Aberration-Free Ultrathin Flat Lenses and Axicons at Telecom Wavelengths Based on Plasmonic Metasurfaces," *Nano Letters*, vol. 12, no. 9, pp. 4932–4936, Aug. 2012, doi: 10.1021/nl302516v.

[22] N. Yu *et al.,* "Light Propagation with Phase Discontinuities: Generalized Laws of Reflection and Refraction," *Science*, vol. 334, no. 6054, pp. 333–337, Sep. 2011, doi: 10.1126/science.1210713.

[23] J. Fan and Y. Cheng, "Broadband high-efficiency cross-polarization conversion and multi-functional wavefront manipulation based on chiral structure metasurface for terahertz wave," *Journal of Physics D: Applied Physics*, vol. 53, no. 2, p. 025109, Oct. 2019, doi: 10.1088/1361-6463/ab4d76.

[24] J. Fan, Y. Cheng, and B. He, "High-efficiency ultrathin terahertz geometric metasurface for full-space wavefront manipulation at two frequencies," *Journal of Physics D: Applied Physics*, vol. 54, no. 11, p. 115101, Jan. 2021, doi: 10.1088/1361-6463/abcdd0.

[25] R. S. Malfajani and Z. Atlasbaf, "Design and Implementation of a Dual-Band Single Layer Reflectarray in X and K Bands," in *IEEE Transactions on Antennas and Propagation*, vol. 62, no. 8, pp. 4425-4431, Aug. 2014, doi: 10.1109/TAP.2014.2327137.

[26] H. Moghadas, M. Daneshmand, and P. Mousavi, "MEMS-Tunable Half Phase Gradient Partially Reflective Surface for Beam-Shaping," in *IEEE Transactions on Antennas and Propagation*, vol. 63, no. 1, pp. 369-373, Jan. 2015, doi: 10.1109/TAP.2014.2364303.

[27] H. Li, G. Wang, H. Xu, T. Cai, and J. Liang, "X-Band Phase-Gradient Metasurface for High-Gain Lens Antenna Application," in *IEEE Transactions on Antennas and Propagation*, vol. 63, no. 11, pp. 5144-5149, Nov. 2015, doi: 10.1109/TAP.2015.2475628.

[28] H. Li, G. Wang, X. Gao, J. Liang, and H. Hou, "A Novel Metasurface for Dual-Mode and Dual-Band Flat High-Gain Antenna Application," in *IEEE Transactions on Antennas and Propagation*, vol. 66, no. 7, pp. 3706-3711, Jul. 2018, doi: 10.1109/TAP.2018.2835526.

[29] X. Zhong, H. Xu, L. Chen, W. Li, H. Wang, and X. Shi, "An FSS-Backed Broadband Phase-Shifting Surface Array with Multimode Operation," in *IEEE Transactions on Antennas and Propagation*, vol. 67, no. 9, pp. 5974-5981, Sep. 2019, doi: 10.1109/TAP.2019.2916747.

[30] H. Yue, L. Chen, Y. Yang, L. He, and X. Shi, "Design and Implementation of a Dual Frequency and Bidirectional Phase Gradient Metasurface for Beam Convergence," in *IEEE Antennas and Wireless Propagation Letters*, vol. 18, no. 1, pp. 54-58, Jan. 2019, doi: 10.1109/LAWP.2018.2880491.

BIOGRAPHIES OF AUTHORS

Devendra Soni is a Ph.D. scholar in Department of Electronics and Communication Engineering, at Manipal University Jaipur, India. He graduated with a Bachelor of Engineering (B.E.) in Electronics and Communication from Ajmer Institute of Technology, Ajmer in 2008. He earned a Master in Technology (M.Tech.) degree in Digital Communication from Arya College of Engineering and Information Technology, Jaipur in 2012. He can be contacted at email: sonierdevendra6486@gmail.com.

Dr. Dinesh Yadav did a B.E. in Electronics and Communication Engineering and M.Tech. in Digital Communication, in 2007 and 2009, respectively. He completed his Ph.D. in "UWB Reconfigurable and MIMO Antennas" in 2018. Presently, he is working as an Associate Professor in the Department of Electronics and Communication Engineering, at Manipal University Jaipur. He is an active member of IEEE AP-S, IEEE MTT-S, IEEE Communication Societies, a Life member of IETE, and a Life member of IE (I). He is also a Senior Member of IEEE (USA). He is an author/co-author of more than 50 research papers in national/International conferences and journals. He can be contacted at email: dinesh.yadav@jaipur.manipal.edu.

Dr. Manish Tiwari received a Ph.D. in ECE in the field of Photonics from MNIT Jaipur. Presently, he is a Professor of ECE at Manipal University Jaipur. He is a Senior Member of the IEEE Photonics Society, Communication Society, Broadcast Technology Society, Antenna and Propagation Society, Life Fellow of the Optical Society of India (OSI-India), Senior Member of OSA, Member of SPIE and Fellow of the Institution of Electronics and Telecommunication Engineers (IETE) India. His current research interests include micro/nano-structure photonic devices, photonic ICs, fiber optics, numerical modelling, nonlinear optics, and photonic crystal fibers. He can be contacted at email: manish.tiwari@jaipur.manipal.edu.